Bacterial Microcompartments Coupled with Extracellular Electron Transfer Drive the Anaerobic Utilization of Ethanolamine in *Listeria monocytogenes*

Zhe Zeng,[a] Sjef Boeren,[b] Varaang Bhandula,[c] Samuel H. Light,[d] Eddy J. Smid,[a] Richard A. Notebaart,[a] (ID) Tjakko Abee[a]

[a]Food Microbiology, Wageningen University and Research, Wageningen, the Netherlands
[b]Laboratory of Biochemistry, Wageningen University and Research, Wageningen, the Netherlands
[c]Department of Molecular and Cell Biology, University of California, Berkeley, Berkeley, California, USA
[d]Department of Microbiology, The University of Chicago, Chicago, Illinois, USA

ABSTRACT Ethanolamine (EA) is a valuable microbial carbon and nitrogen source derived from cell membranes. EA catabolism is suggested to occur in a cellular metabolic subsystem called a bacterial microcompartment (BMC), and the activation of EA utilization (*eut*) genes is linked to bacterial pathogenesis. Despite reports showing that the activation of *eut* is regulated by a vitamin B_{12}-binding riboswitch and that upregulation of *eut* genes occurs in mice, it remains unknown whether EA catabolism is BMC dependent in *Listeria monocytogenes*. Here, we provide evidence for BMC-dependent anaerobic EA utilization via metabolic analysis, proteomics, and electron microscopy. First, we show vitamin B_{12}-induced activation of the *eut* operon in *L. monocytogenes* coupled to the utilization of EA, thereby enabling growth. Next, we demonstrate BMC formation connected with EA catabolism with the production of acetate and ethanol in a molar ratio of 2:1. Flux via the ATP-generating acetate branch causes an apparent redox imbalance due to the reduced regeneration of NAD^+ in the ethanol branch resulting in a surplus of NADH. We hypothesize that the redox imbalance is compensated by linking *eut* BMCs to anaerobic flavin-based extracellular electron transfer (EET). Using *L. monocytogenes* wild-type, BMC mutant, and EET mutant strains, we demonstrate an interaction between BMCs and EET and provide evidence for a role of Fe^{3+} as an electron acceptor. Taken together, our results suggest an important role of BMC-dependent EA catabolism in *L. monocytogenes* growth in anaerobic environments like the human gastrointestinal tract, with a crucial role for the flavin-based EET system in redox balancing.

IMPORTANCE *Listeria monocytogenes* is a foodborne pathogen causing severe illness, and as such, it is crucial to understand the molecular mechanisms contributing to pathogenicity. One carbon source that allows *L. monocytogenes* to grow in humans is ethanolamine (EA), which is derived from phospholipids present in eukaryotic cell membranes. It is hypothesized that EA utilization occurs in bacterial microcompartments (BMCs), self-assembling subcellular proteinaceous structures and analogs of eukaryotic organelles. Here, we demonstrate that BMC-driven utilization of EA in *L. monocytogenes* results in increased energy production essential for anaerobic growth. However, exploiting BMCs and the encapsulated metabolic pathways also requires the balancing of oxidative and reductive pathways. We now provide evidence that *L. monocytogenes* copes with this by linking BMC activity to flavin-based extracellular electron transfer (EET) using iron as an electron acceptor. Our results shed new light on an important molecular mechanism that enables *L. monocytogenes* to grow using host-derived phospholipid degradation products.

Pathogens have evolved mechanisms to utilize specific metabolites as carbon sources to sidestep nutritional competition with commensal bacteria in the human gastrointestinal (GI) tract (1–4). Ethanolamine (EA), a product of the breakdown of phosphatidylethanolamine from eukaryotic cell membranes, is such a metabolite and is abundant in the human GI tract (5, 6). It has been shown that some species in the GI tract, like *Salmonella enterica*, *Enterococcus faecalis*, and *Clostridium perfringens*, can use EA as a carbon source, while for some other human pathogens, including *Listeria monocytogenes*, the putative use of EA as a substrate was postulated based on the presence of a similar gene cluster (5–7). The ability to utilize EA is encoded by the ethanolamine utilization (*eut*) operon (6–8). EA is converted to acetaldehyde and ammonia by the ethanolamine ammonia lyase EutBC (6, 9, 10). Acetaldehyde can be catabolized to ethanol by the alcohol dehydrogenase EutG (8) or to acetyl-CoA by the acetaldehyde dehydrogenase EutE (6, 11). Acetyl-CoA can be degraded to acetate with ATP production by the phosphotransacetylase EutD (12) and an alternative acetate kinase, EutQ (13). Alternatively, acetyl-CoA can be catabolized in the tricarboxylic acid cycle or the glyoxylate cycle or used for lipid biosynthesis (6). According to current models, EA is catabolized to acetate and ethanol in a molar ratio of 1:1 via the oxidative ATP-producing branch and reductive NAD^+-regenerating branch (6). Interestingly, previous studies showed that EA confers a marked anaerobic growth advantage on *Salmonella enterica* serovar Typhimurium only in the presence of tetrathionate, acting as an alternative electron acceptor via tetrathionate reductase (6, 14–16), and the mutant lacking the tetrathionate reductase showed a decreasing colonization capacity in a mouse colitis model, which points to a role for anaerobic electron transfer in EA catabolism contributing to the growth of *S. enterica* in the lumen of the inflamed intestine (15). Anaerobic EA catabolism in *L. monocytogenes*, including possible roles for anaerobic respiration, has not been studied. Notably, *L. monocytogenes* lacks tetrathionate reductase, but anaerobic electron transfer with fumarate reduction via membrane-bound fumarate reductase (17) and the recently described flavin-based extracellular electron transfer (EET) with Fe^{3+} as an electron acceptor (18) could act as substitutes in bacterial microcompartment (BMC)-dependent EA catabolism.

The enzymes of the indicated EA pathway are present in a BMC, and structural shell proteins that constitute the BMC building blocks are encoded by genes in the *eut* cluster (19). BMCs consist of a capsule of semipermeable shell proteins and encapsulated enzymes of metabolic pathways that liberate toxic intermediates in the lumen of the capsules (19–21). In the formation of BMCs, so-called encapsulation peptides, 10- to 20-residue-long hydrophobic α-helices in the N termini of some core enzymes, play a key role in the encapsulation mechanism (22, 23). In our previous study, evidence was provided for a role of BMC-dependent utilization of 1,2-propanediol in *L. monocytogenes* supporting anaerobic growth and metabolism, and the encapsulated enzymes PduD, PduL, and PduP were found to contain encapsulation peptides (24). Expression of the *eut* operon in *L. monocytogenes* is under the regulation of the two-component regulators EutVW sequestrated by a vitamin B_{12}-binding riboswitch (25, 26). Upregulation of the *eut* operon has been found in *L. monocytogenes* grown on vacuum-packed cold-smoked salmon and in cocultures with cheese rind bacteria, which suggests a possible role of the *eut* operon in the adaptation of *L. monocytogenes* to available nutrient sources (27, 28). The *L. monocytogenes eut* operon exhibited increased expression inside the host cell, and the loss of one of the key enzymes, ethanolamine ammonia lyase (EutB), caused a defect in intracellular growth (29).

Here, we show by using metabolic analysis, transmission electron microscopy (TEM), and proteomics that *L. monocytogenes* forms *eut* BMCs and utilizes EA as a carbon source under anaerobic conditions with the end products acetate and ethanol in a molar ratio of 2:1. We demonstrate that the resulting redox imbalance is compensated by the flavin-based EET system by comparative growth and metabolic analyses of *L. monocytogenes* wild-type, BMC mutant, and EET mutant strains. Our results suggest an
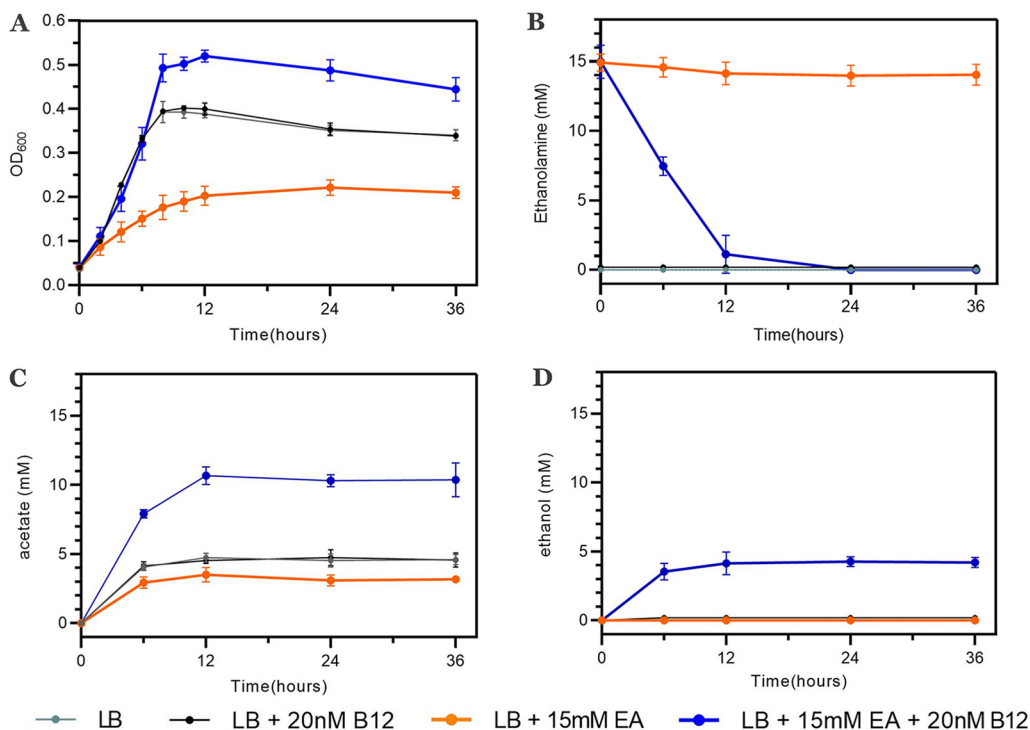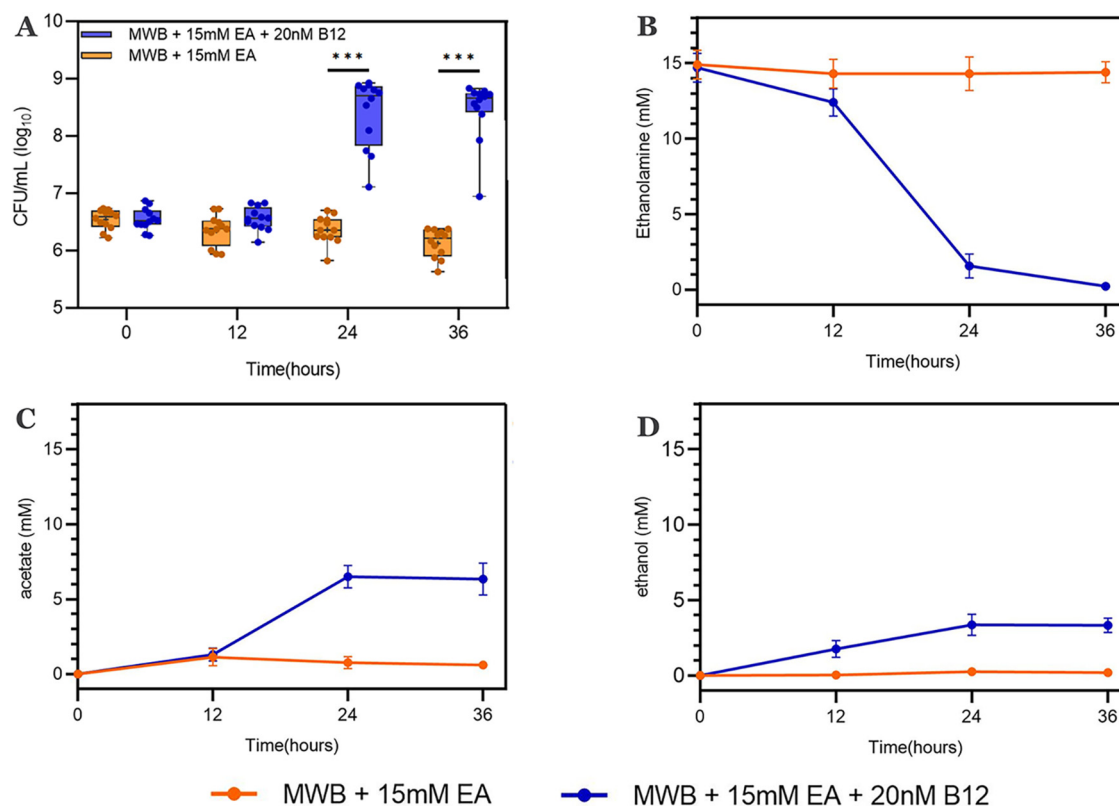
FIG 1 Anaerobic growth and EA catabolism of *L. monocytogenes* EGDe in LB medium. (A) Impact of EA and/or vitamin B$_{12}$ on anaerobic growth of *L. monocytogenes* EGDe; (B) EA utilization; (C) acetate production; (D) ethanol production. Lines represent different growth conditions. Results from three independent experiments are expressed and visualized as means and standard errors.

important role of anaerobic BMC-dependent EA catabolism in the physiology of *L. monocytogenes*, with a crucial role for the flavin-based EET system in redox balancing.

RESULTS

EA utilization facilitates anaerobic growth. To find out whether EA utilization stimulates anaerobic growth, we added EA (15 mM) to Luria broth (LB) medium in line with previous work in *Salmonella* species (11, 30). The culture medium also contained 20 nM vitamin B$_{12}$ for the activation of the *eut* operon in *L. monocytogenes* (25). *L. monocytogenes* EGDe cultures grown under *eut*-induced conditions (LB with EA and B$_{12}$) reached significantly higher optical density at 600 nm (OD$_{600}$) values after 8 h of incubation than cultures under control conditions (LB and LB with B$_{12}$) and those under *eut*-noninduced conditions (LB with EA) (Fig. 1A). EA under *eut*-induced conditions was fully utilized within the first 24 h, while no significant EA utilization was observed under *eut*-noninduced conditions (Fig. 1B). Notably, under *eut*-induced conditions, EA was converted into acetate and ethanol (Fig. 1C and D), while under *eut*-noninduced conditions, only acetate was produced, conceivably originating from the metabolism of other compounds in LB. From this comparative analysis of acetate production, we derive a molar ratio of acetate to ethanol of approximately 2:1. Taken together, the utilization of EA with the production of acetate and ethanol contributes to the anaerobic growth of *L. monocytogenes* EGDe under *eut*-induced conditions.

Ratio of ethanol to acetate production. To clarify whether *L. monocytogenes* EGDe can utilize EA as a sole carbon source, we examined EA utilization and its impact on anaerobic growth in the defined medium Modified Welshimer's broth (MWB) in the absence of any other carbon sources (31). *L. monocytogenes* EGDe inoculated under *eut*-induced conditions (MWB with EA and vitamin B$_{12}$) showed an ~100-fold increase in cell counts after 24 h, while no significant increase in cell counts was observed under noninduced conditions (MWB with EA) (Fig. 2A). Microscopy analysis of samples

FIG 2 Anaerobic growth and EA catabolism of *L. monocytogenes* EGDe in MWB defined medium with EA as the sole carbon source. (A) Impact of EA and/or vitamin B$_{12}$ on CFU of *L. monocytogenes* EGDe. Results from three independent experiments with four technical repeats are expressed as means and standard errors. Statistical significance is indicated (***, $P < 0.001$ [by a Holm-Sidak t test]). (B) EA utilization. (C) Acetate production. (D) Ethanol production. Cells were grown in MWB plus 15 mM EA without B$_{12}$ and with 20 nM B$_{12}$. Error bars in panels B to D indicate results from three independent experiments expressed as means and standard errors.

showed the absence of chains of cells, excluding the option that the increase in CFU is due to the disintegration of chains of cells. During the anaerobic growth of *L. monocytogenes* EGDe, 15 mM EA was converted into about 6.6 mM acetate and 3.4 mM ethanol under *eut*-induced conditions, while no significant degradation of EA was observed under noninduced conditions (Fig. 2B to D). Through calculation of the carbon mass balance, part of EA (approximately 5 mM) is conceivably further catabolized in the γ-aminobutyrate (GABA) shunt (32) or used for lipid biosynthesis via the intermediate acetyl-CoA (6). The utilization of EA under *eut*-induced conditions in the defined medium MWB provides evidence that EA can act as a sole carbon source supporting the anaerobic growth of *L. monocytogenes* EGDe. Notably, the observed molar ratio of acetate to ethanol of 2:1 suggests an apparent redox imbalance due to higher flux via the NADH- and ATP-producing acetate branch and reduced regeneration of NAD$^+$ in the ethanol branch resulting in a surplus of NADH.

Upregulated expression of the *eut* operon, including enzymes and structural shell proteins. In order to study the expression of the *eut* operon and the way in which it is embedded in cell physiology, we performed proteomics to compare *L. monocytogenes* cells grown in LB and MWB medium under *eut*-induced conditions and noninduced conditions. Analyses of the complete list of identified proteins, the proteins' expression levels, and subsequent t test results and P values are shown in Table S2 in the supplemental material for LB-grown and in Table S3 for MWB-grown cells. For LB, we identified 1,891 total proteins where 161 proteins are upregulated more than 2-fold and 229 proteins are downregulated more than 2-fold under *eut*-induced conditions compared to noninduced conditions (Fig. 3A). Among these 161
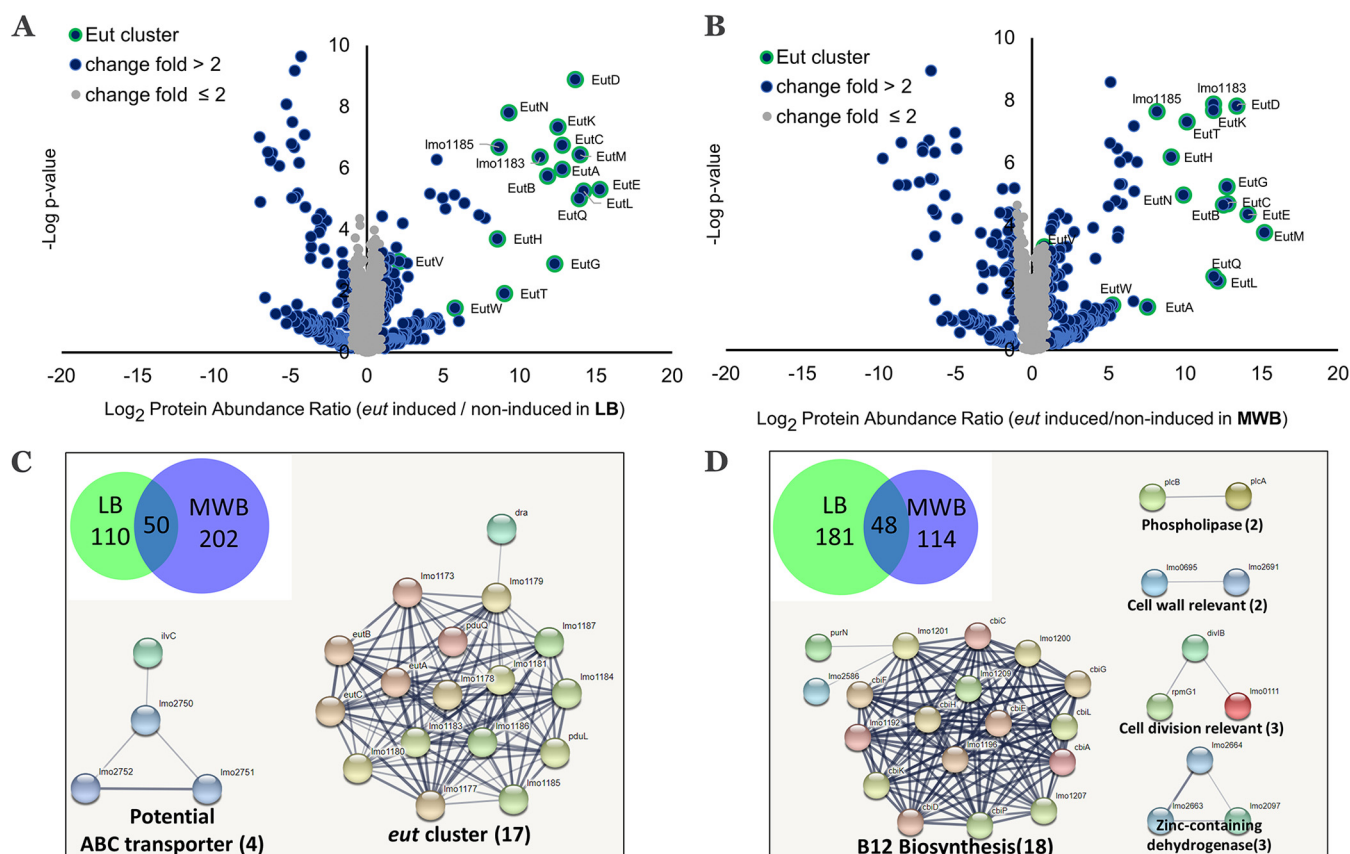
FIG 3 Proteomics analysis of *eut*-induced and noninduced *L. monocytogenes* EGDe in LB medium and MWB defined medium. (A and B) Proteomic volcano plot of *eut*-induced cells (EA and vitamin B$_{12}$ added) compared to noninduced cells (EA added only) in LB medium (A) and MWB medium (B). (C and D) Venn diagram of 50 overlapping upregulated proteins (C) 48 overlapping downregulated proteins (D) for LB medium (green) and MWB medium (blue) and corresponding STRING protein-protein interactions. Nodes represent proteins, and lines represent interactions.

upregulated proteins, the top 15 proteins are all encoded in the *eut* operon, i.e., EutGABCLKEMTDNHQ, lmo1183, and lmo1185, while the other two proteins, EutVW (33), involved in *eut* operon regulation are also included. For MWB, 1,736 proteins were identified, of which 253 proteins are upregulated more than 2-fold and 162 proteins are downregulated more than 2-fold under *eut*-induced conditions compared to non-induced conditions (Fig. 3B). In line with the LB data, the top 15 proteins are all encoded in the *eut* operon. Analysis of the upregulated proteins in LB and MWB media shows 50 proteins that overlap between the conditions, pointing to a prominent role under *eut*-induced conditions compared to noninduced conditions. Among these 50 proteins, 17 proteins are linked to *eut*, of which 16 proteins are encoded in the *eut* operon, and one gene, *dra* (deoxyribose-phosphate aldolase), is predicted to have an interaction with the acetaldehyde dehydrogenase *eutE* (lmo1179) (according to STRING analysis) (Fig. 3C; Table S4). Another group of overlapping genes comprises potential ABC transporters, including *lmo2751-lmo2752* (ABC transporter ATP-binding protein) (34), and *ilvC* (*lmo1986*) (NADP$^+$-based ketol acid reductoisomerase) (35). The analysis of downregulated proteins in LB and MWB showed an overlap of 48 proteins, with 18 proteins linked to vitamin B$_{12}$ biosynthesis, which indicates that adding vitamin B$_{12}$ to the medium represses the genes involved in vitamin B$_{12}$ biosynthesis (Fig. 3D; Table S5). The overlap in downregulated proteins also showed enrichment in phospholipases (*plcA* and *plcB*), putative cell wall-relevant proteins (*lmo2691* [putative peptidoglycan hydrolase autolysin] and *lmo0695* [similar to the flagellar hook length control protein FliK]), cell division-relevant proteins (*dilvB*, *rpmG1*, and *lmo0111*) (Table S5), and zinc-containing dehydrogenases (*lmo2663*, *lmo2664*, and *lmo2097*). To summarize, the significant upregulation of the *eut* operon at the proteomic level, including structural
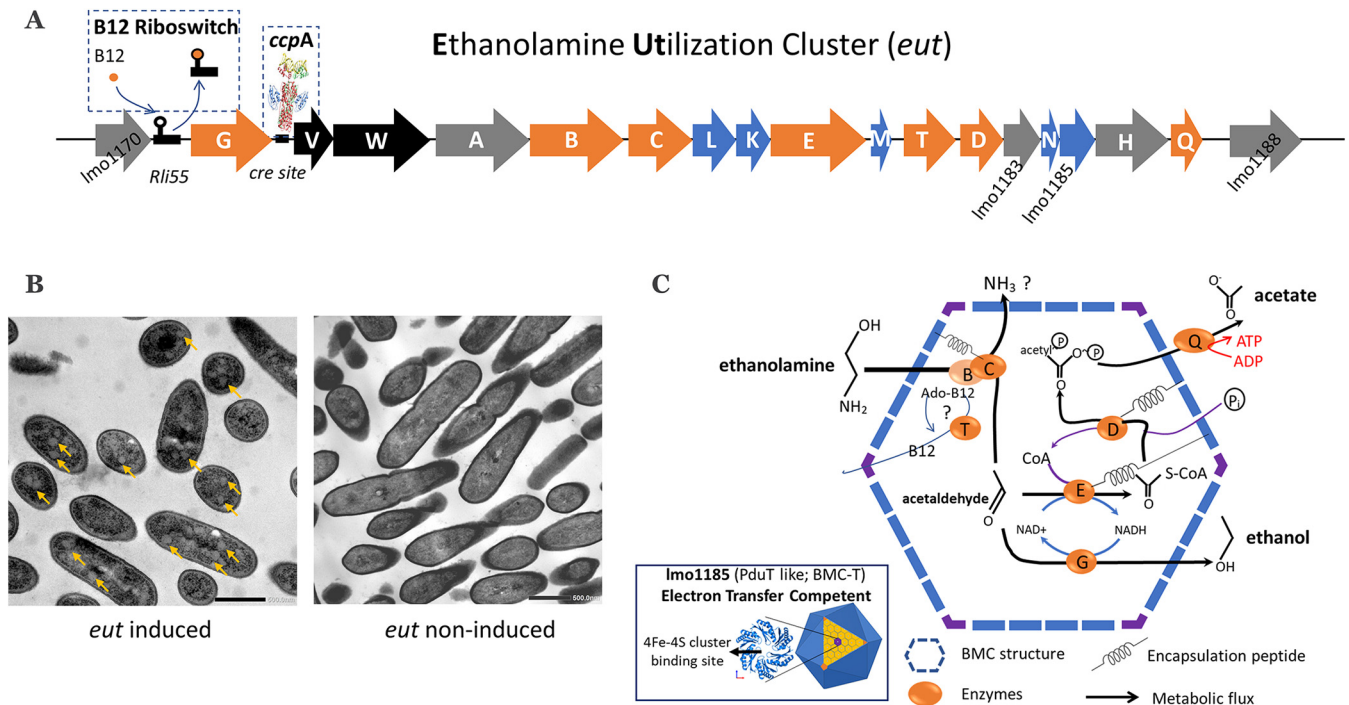
FIG 4 Overview of the BMC-dependent EA catabolism model of *L. monocytogenes*. (A) Analysis of the *eut* operon (for details, see Table S1 in the supplemental material). Characters in orange represent Eut enzymes, those in blue represent BMC shell proteins, those in black represent the two-component regulation system, and those in gray represent unannotated proteins. The vitamin B_{12} riboswitch and CcpA *cre*-binding site are indicated. (B) TEM visualization of BMCs in *eut*-induced (left) (yellow arrows point to BMCs) and noninduced (right) cells. (C) Model of BMC-dependent EA catabolism. EutBC, ethanolamine ammonia lyase; EutD, phosphotransacetylase; EutE, acetaldehyde dehydrogenase; EutG, alcohol dehydrogenase; EutQ, acetate kinase; EutT, corrinoid cobalamin adenosyltransferase. Putative encapsulation peptides are indicated. The zoomed-in part shows the prediction of the potential [4Fe-4S] cluster-binding site in Eut shell protein lmo1185, which is highly similar to that previously reported for the PduT shell protein by Pang et al. (39). See the text for details.

shell proteins, strongly supports that BMC-dependent EA utilization is processed by enzymes and structural shell proteins of the *eut* operon.

BMC structures support BMC-dependent EA catabolism. To further confirm the presence of BMCs in *eut*-induced cells, we used transmission electron microscopy (TEM) and compared thin sections of both *eut*-induced and noninduced *L. monocytogenes* EGDe cells. The *eut*-induced cells clearly contain BMC-like structures with a diameter of approximately 50 to 80 nm, which are not present in noninduced cells (Fig. 4B). Notably, the identified structures strongly resemble those in TEM pictures of BMCs in *S. enterica* and *Escherichia coli* (36, 37) and that of recently reported BMCs found in *pdu*-induced *L. monocytogenes* (24). Taking the metabolic, proteomic, and TEM data together, we conclude that the cytosolic BMC-like structures in *L. monocytogenes* EGDe are involved in EA utilization under anaerobic conditions. Here, based on the knowledge of the *eut* operon, we propose a model of BMC-dependent EA catabolism. The *eut* operon in *L. monocytogenes* EGDe contains 17 genes and is most likely under the regulation of the two-component regulators EutVW sequestered by the binding of vitamin B_{12} to the riboswitch rli55 (25). In front of EutVW, we found a previously predicted *cre* site for the binding of the carbon control protein CcpA, pointing to catabolite repression control of the *L. monocytogenes eut* cluster (38). Five *eut* genes, *eutLKMN* and *lmo1185*, are predicted to be structural shell proteins of the BMC (Fig. 4A). EutK and EutM are the hexameric shell protein (BMC-H) consisting of one Pfam00936 domain, while EutL and lmo1185 are the trimeric shell proteins (BMC-T) with two fused Pfam00936 domains (Fig. S1). Notably, the trimeric assembly of lmo1185 forms a flat approximately hexagonally shaped disc with a central pore that is suitable for a [4Fe-4S] cluster (39). Furthermore, EutN is the pentameric shell protein (BMC-P) consisting of one Pfam03319 domain (Fig. S1). The BMC is assembled by these three types of shell proteins, BMC-H, BMC-T, and BMC-P (19, 20). Based on the previous BMC-dependent
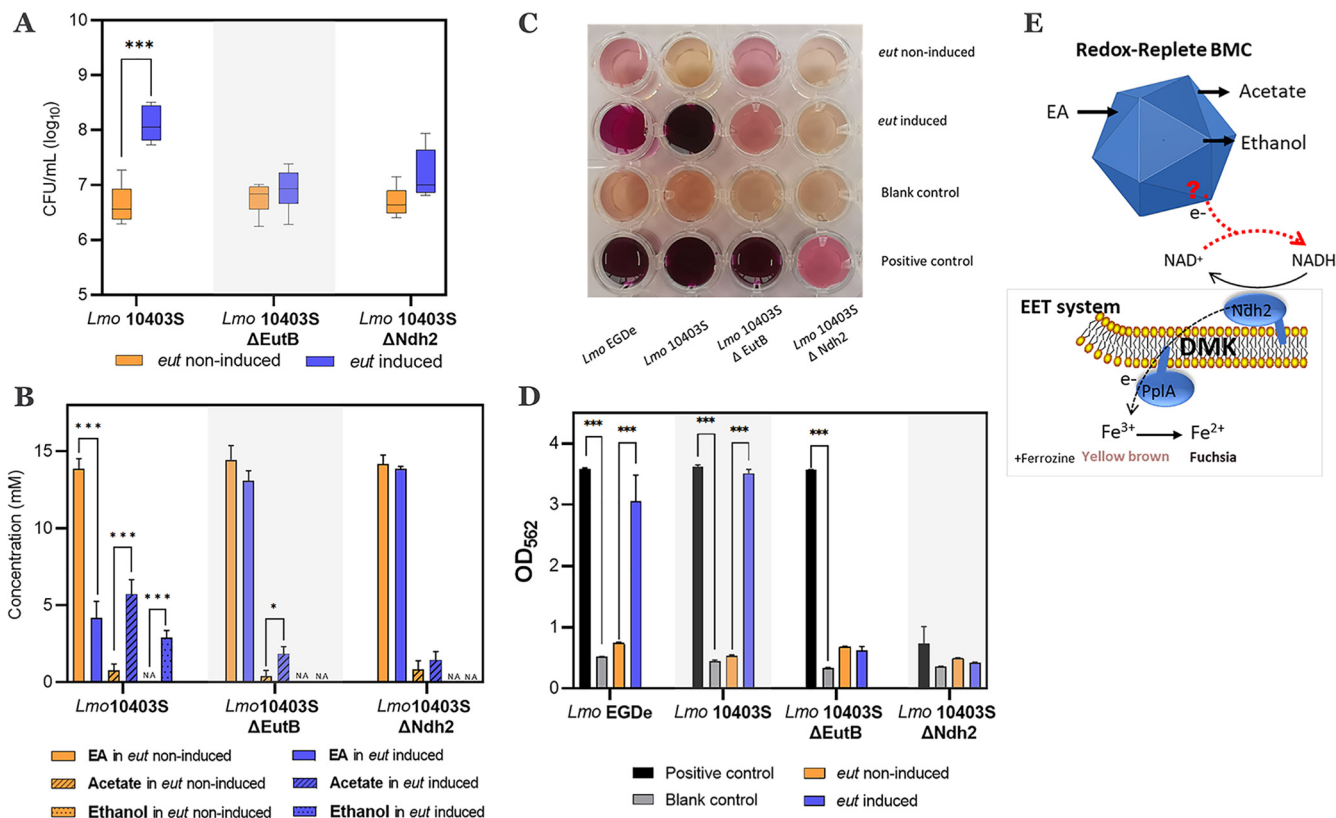
FIG 5 BMC-dependent EA catabolism is coupled to flavin-based EET. (A) Impact of EA and/or vitamin B_{12} on CFU. (B) EA catabolism. Experiments in panels A and B were performed with *L. monocytogenes* 10403S and mutant strains grown anaerobically for 24 h with an initial inoculum of 6.5 ± 0.1 $\log_{10}$ CFU/ml in MWB with 15 mM EA and 20 nM B_{12} (*eut* induced) or 15 mM EA (noninduced). (C) Colorimetric change of the ferric reductase assay. (D) OD_{562} measurements of the ferric reductase assay. Experiments in panels C and D were performed with *L. monocytogenes* EGDe, 10403S, and mutant strains grown anaerobically for 24 h in MWB with 15 mM EA and 20 nM B_{12} (*eut* induced), 15 mM EA (noninduced), 15 mM glucose (positive control), or no added substrate (blank control). Results in panels A, B, and D are from three independent experiments and are expressed as means and standard errors. Statistical significance is indicated (***, $P < 0.001$; *, $P < 0.05$ [by a Holm-Sidak *t* test]). (E) Proposed model of electron transfer from the BMC to the EET system. The blue geometric block represents the BMC. CM represents the cytoplasmic membrane. Ndh2, PplA, and DMK (demethylmenaquinone) represent EET with Fe^{3+} as an electron acceptor (see the text for details).

EA catabolism model in *S. enterica* (5), we propose a model for *L. monocytogenes* with putative encapsulation peptides supporting the recruitment of selected Eut enzymes to the BMC (Fig. 4C). We predict a specific hydrophobic α-helix in the N terminus of the encapsulated enzymes EutC, EutD, and EutE (Fig. S2), similar to those of the previously described BMC-encapsulated proteins in *S. enterica* and *pdu* BMCs in *L. monocytogenes* (22, 24). EA is split into acetaldehyde and ammonia by the ethanolamine ammonia lyase EutBC (6, 9, 10). Acetaldehyde can be converted into ethanol by the alcohol dehydrogenase EutG (8) or into acetyl-CoA by the acetaldehyde dehydrogenase EutE (6, 11). Acetyl-CoA can be converted into acetyl-phosphate and subsequently acetate and ATP by the phosphotransacetylase EutD (12) and an alternative acetate kinase, EutQ, respectively (13).

Flavin-based EET linked with BMCs maintains redox balance of EA catabolism. The observed unbalanced production of acetate and ethanol in a 2:1 molar ratio suggests a surplus of NADH, and this requires additional NAD⁺ regeneration reactions to restore the redox balance. As discussed above, the BMC is a redox-replete compartment that can generate reductants internally or facilitate the transfer of electrons from the cytosol across the shell (6, 40). Recently, it has been shown that *L. monocytogenes* uses a distinctive anaerobic flavin-based EET mechanism to deliver electrons to iron (Fe^{3+}) or to fumarate via membrane-bound fumarate reductase (18). In our study, MWB defined medium indeed contains ferric citrate and flavin, and proteomic analysis of *L. monocytogenes* EGDe grown in this medium identified *lmo2637* encoding an EET-

linked lipoprotein, PplA, and *lmo2638*, encoding an EET-linked NADH dehydrogenase, Ndh2 (18) (Table S3). Next, we tested the hypothesis that anaerobic EET could play a role in BMC-dependent EA utilization using *L. monocytogenes* 10403S wild-type and mutant strains. Notably, *eut*-induced *L. monocytogenes* 10403S showed a growth benefit from utilizing EA similar to that of *eut*-induced *L. monocytogenes* EGDe (Fig. 5A and B). Moreover, the mutant strains *L. monocytogenes* 10403S Δ*eutB*, lacking ethanolamine ammonia lyase, and Δ*ndh2*, lacking EET-linked NADH dehydrogenase, are both impaired for EA utilization (Fig. 5B), suggesting an involvement of the EET system in EA utilization and thereby a link with BMCs. Next, we used a ferrozine-based colorimetric assay to determine electron transfer between the BMC and the EET system following *L. monocytogenes* EA utilization in MWB medium. In this assay, electrons generated from EA catabolism are transferred to Fe^{3+}, generating Fe^{2+}, where the binding of ferrozine to the differently charged Fe molecules results in a colorimetric change from yellow-brown to fuchsia, respectively. The colorimetric changes were shown for *L. monocytogenes* EGDe and *L. monocytogenes* 10403S under *eut*-induced conditions following EA utilization, while *eut* mutant strain *L. monocytogenes* 10403S Δ*eutB* and EET mutant strain *L. monocytogenes* 10403S Δ*ndh2* showed no colorimetric changes (Fig. 5C). OD_{562} measurements indicated significantly higher ferric iron reductase activity under *eut*-induced conditions than under noninduced conditions for *L. monocytogenes* EGDe and *L. monocytogenes* 10403S (Fig. 5D). Taken together, these results provide evidence for a link between *eut* BMCs and the EET system via the regeneration of NAD^+ by NADH oxidation in EET using Fe^{3+} as an electron acceptor (Fig. 5E). The action of EET as an alternative reductive pathway next to the ethanol branch thus stimulates anaerobic growth by enhanced flux via the ATP-generating acetate branch in BMC-facilitated EA catabolism.

DISCUSSION

This study provides evidence for the activation of BMC-dependent ethanolamine (EA) utilization in *L. monocytogenes* under anaerobic conditions in LB and MWB medium containing EA and vitamin B_{12}. By using metabolic analysis, proteomics, and electron microscopy, we demonstrated the formation of BMCs in conjunction with EA catabolism with the production of acetate and ethanol in a 2:1 molar ratio. Selected genes in the *eut* operon encode structural shell proteins that form the respective *eut* BMCs (19). Previous studies showed that BMCs for EA catabolism in *S. enterica* and *E. faecalis* are composed of five structural shell proteins, EutS, EutM, EutK, EutL, and EutN (6, 19, 21). Notably, the *L. monocytogenes eut* operon also encodes five putative shell proteins, EutM, EutK, EutL, EutN, and lmo1185, and combined with the visualization of BMC structures by TEM and our proteomic data, we conclude that *eut* BMCs are composed of these five indicated structural shell proteins. Apparently, EutS is not essential for BMC assembly in *L. monocytogenes*. EutS is hexameric BMC shell protein with a Pfam00936 domain, and it is conceivable that the function of EutS is taken over by EutK and/or EutM in *L. monocytogenes* since both proteins are also hexameric BMC shell proteins with a Pfam00936 domain (see Fig. S1 in the supplemental material).

EA is a valuable carbon source for *L. monocytogenes* to outcompete other bacteria unable to utilize EA in food environments (27, 28) or the human GI tract, where EA is abundant (5, 6). Our results in defined medium reveal that *L. monocytogenes* can utilize EA as a sole carbon source via a BMC-dependent *eut* pathway (Fig. 2). Encasing the pathway inside BMCs is essential since this prevents the toxic acetaldehyde intermediate from damaging proteins and RNA/DNA in the cytoplasm (19, 41). The generated reductants are oxidized inside the BMC, while it has been hypothesized that electrons may also be shuttled to the cytosol via specific shell proteins acting as redox carriers (6, 19, 20, 40). Our metabolite analysis showed enhanced flux via the ATP-generating acetate branch in *L. monocytogenes* and reduced flux via the NAD^+-regenerating ethanol branch in a 2:1 molar ratio resulting in surplus NADH. In support of the above-mentioned putative electron shuffling from BMCs to the cytosol, using wild-type, EutB

mutant, and Ndh2 mutant strains, we identified a link between *L. monocytogenes eut* BMC activity and the recently discovered flavin-based EET system (Fig. 5E) (18). The suggested electron acceptors fumarate and iron are conceivably present in the human intestine and in host cells and have been reported to contribute to *L. monocytogenes* virulence (17, 18, 42, 43). The identified *L. monocytogenes eut* lmo1185 shell protein belongs to the class of trimeric shell proteins (BMC-T) with two fused Pfam00936 domains. We hypothesize that this predicted PduT-like shell protein with a [4Fe-4S] cluster (39) acts as a redox carrier in this process. Further studies are required to elucidate the role of this *eut* BMC shell protein as a redox carrier.

Taken together, our results provide evidence of anaerobic EA catabolism in *L. monocytogenes* driven by BMC formation and function, with a crucial role for the flavin-based EET system in redox balancing. These findings provide a new model (Fig. 5E) involving two interconnected cellular subsystems that explains how *L. monocytogenes* is able to grow and adapt in EA-rich environments like the human GI tract.

MATERIALS AND METHODS

Strains, culture conditions, and growth measurements. All *L. monocytogenes* strains used in this study are shown in Table S6 in the supplemental material. *L. monocytogenes* strains were anaerobically grown at 30°C in Luria broth (LB) medium and the defined medium MWB (31). LB and MWB were supplemented with 15 mM EA and/or 20 nM vitamin B_{12} (25). Anaerobic conditions were achieved by using an Anoxomat anaerobic culture system with an environment of 10% CO_2, 5% H_2, and 85% N_2. LB and MWB with 15 mM EA and 20 nM vitamin B_{12} were defined as *eut*-induced conditions, while LB and MWB with 15 mM EA were defined as noninduced conditions. OD_{600} measurements in LB were performed every 2 h during the first 12 h of incubation and at 24 and 36 h. Plate counting in MWB to quantity CFU was performed every 12 h from 0 h to 36 h.

Construction of strain *L. monocytogenes* 10403S Δ*eutB*. The *L. monocytogenes* Δ*eutB* strain was derived from wild-type strain 10403S (DP-L6253). Gene deletions were generated by allelic exchange using the plasmid pKSV7 (44) with a chloramphenicol resistance gene. Primers used for Δ*eutB* fragment construction and validation of the deletion are given in Table S7. Fragment A and fragment B flanking the *eutB* gene were ligated into the plasmid using Gibson assembly and cloned in *E. coli* Top10. The plasmid construct was verified by Sanger sequencing. The plasmid was then transformed into *E. coli* SM10. Transconjugation was performed to integrate the plasmid using a restrictive temperature of 42°C, and colonies that were resistant to streptomycin (200 μg/ml) and chloramphenicol (7.5 μg/ml) were selected. This was followed by passaging in brain heart infusion broth at 37°C with shaking, diluting 1:1,000 every 8 h. The mutant was obtained by screening for chloramphenicol-sensitive colonies followed by colony PCR using validation primers.

Analysis of metabolites for EA catabolism. After centrifugation, the supernatants of the cultures were collected and filtered with a 0.45-μm syringe filter for the measurements. EA (monoethanolamine) at a 1:1 dilution in ethanol was measured by gas chromatography with flame ionization detection (GC-FID), while ethanol and acetate were directly measured by high-pressure liquid chromatography (HPLC). The experiment was performed twice, with three technical replicates per experiment. Additionally, the standard curves of EA, ethanol, and acetate were measured in the concentration range of 0.1, 1, 5, 10, and 15 mM. HPLC was performed as described previously (24). GC-FID conditions for the final method were as follows: a 0.3-μl injection volume, a 260°C injector temperature, an 1177 injector, an SGE column (BP5, Melbourne, Victoria, Australia) focus liner, a 1:10 split, a 335°C detector temperature, and an electronic flow controller delivering 2.8 ml/min helium carrier gas with a 2.0-lb/in^2 pressure pulse for 0.25 min after injection. The retention time of EA was 11 min, and the total run time was 50 min (45).

Proteomics. *L. monocytogenes* EGDe cultures were anaerobically grown at 30°C under *eut*-induced and in noninduced conditions. Samples were collected at 12 h for LB and at 24 h for MWB to obtain early-stationary-phase cells. The samples were then washed twice with 100 mM Tris (pH 8). About 10 mg (wet weight) of cells in 100 μl 100 mM Tris was sonicated for 30 s twice to lyse the cells. Samples were prepared according to the filter-assisted sample preparation (FASP) protocol (46). Each prepared peptide sample was analyzed by injecting 18 μl into a nanoscale liquid chromatography-tandem mass spectrometry (nanoLC-MS/MS) system (Thermo nLC1000 instrument connected to an LTQ-Orbitrap XL instrument) (24). LC-MS data with all MS/MS spectra were analyzed with the MaxQuant quantitative proteomics software package as described previously (47). A protein database with the protein sequences of *L. monocytogenes* EGDe (UniProt identifier UP000000817) was downloaded from UniProt. Filtering and further bioinformatics and statistical analyses of the MaxQuant ProteinGroups file were performed with Perseus (48). Reverse hits and contaminants were filtered out. Protein groups were filtered to contain minimally two peptides for protein identification, of which at least one is unique and at least one is unmodified. Also, each group (*eut*-induced and noninduced control groups) required three valid values in at least one of the two experimental groups. The volcano plot was prepared based on the Student's *t* test difference of *eut*-induced/noninduced groups.

Transmission electron microscopy. *L. monocytogenes* EGDe cultures were grown anaerobically at 30°C under *eut*-induced or noninduced conditions. Samples were collected at 12 h of incubation for LB

(early stationary phase). About 10 μg (dry weight) of cells was fixed for 2 h in 2.5% (vol/vol) glutaralde-hyde in 0.1 M sodium cacodylate buffer (pH 7.2). After rinsing in the same buffer, postfixation was done in 1% (wt/vol) OsO_4 for 1 h at room temperature. The samples were dehydrated by ethanol and then embedded in resin (Spurr HM20) for 8 h at 70°C. Thin sections (<100 nm) of polymerized resin samples were obtained with microtomes. After staining with 2% (wt/vol) aqueous uranyl acetate, the samples were analyzed with a Jeol 1400 plus TEM with the 120-kV setting.

Ferrozine assay of ferric iron reductase activity. *L. monocytogenes* cells grown overnight in LB me-dium were washed with phosphate-buffered saline (PBS) twice, normalized to an OD_{600} of 0.2, and resus-pended in fresh MWB medium supplemented with 50 mM ferric ammonium citrate for anaerobic inocu-lation. *L. monocytogenes* wild-type and mutant strains grew anaerobically for 24 h in MWB with 15 mM EA and 20 nM vitamin B_{12} (*eut* induced), 15 mM EA (noninduced), 15 mM glucose (positive control), or no added substrate (blank control). Assays were initiated by adding 100 μl of MWB cultures from a 24-h an-aerobic inoculation to 100 μl demineralized (demi) water with 4 mM ferrozine, and cultures were then spectrophotometrically measured by the OD_{562} as described previously (18). OD_{562} measurements were made immediately after the initial mixture of MWB cultures and ferrozine.

Bioinformatics analysis. (i) Secondary structure of N-terminal peptides. The N-terminal second-ary structures of all *eut* genes were determined by a neural network secondary structure prediction server called Jpred4 (49), as described previously (24). The input to the Jpred4 online server was the 50 N-terminal amino acids of each protein. Jnetconf is the confidence estimation for the prediction, with high scores indicating high confidence. Jnetsol25 is solvent accessibility, where B means buried and "−" means nonburied at a 25% cutoff.

(ii) Venn analysis and STRING networks analysis of proteins. The protein identifiers of signifi-cantly changed proteins from Tables S4 and S5 were uploaded to the BioVenn online server (50) with the default setting to generate Venn diagrams. Overlapping proteins from the Venn diagram were trans-ferred to the STRING online server (51) for multiple-protein analysis of functional interactions using sour-ces such as coexpression, genomic neighborhood, and gene fusion.

SUPPLEMENTAL MATERIAL

Supplemental material is available online only.

FIG S1, DOCX file, 0.4 MB.

FIG S2, DOCX file, 0.5 MB.

TABLE S1, XLSX file, 0.01 MB.

TABLE S2, XLSX file, 0.1 MB.

TABLE S3, XLSX file, 0.1 MB.

TABLE S4, XLSX file, 0.01 MB.

TABLE S5, XLSX file, 0.01 MB.

TABLE S6, DOCX file, 0.01 MB.

TABLE S7, DOCX file, 0.01 MB.

REFERENCES

1. Ley RE, Peterson DA, Gordon JI. 2006. Ecological and evolutionary forces shaping microbial diversity in the human intestine. Cell 124:837–848. https://doi.org/10.1016/j.cell.2006.02.017.

2. Bäumler AJ, Sperandio V. 2016. Interactions between the microbiota and pathogenic bacteria in the gut. Nature 535:85–93. https://doi.org/10.1038/nature18849.

3. Luzader DH, Kendall MM. 2016. Commensal 'trail of bread crumbs' pro-vide pathogens with a map to the intestinal landscape. Curr Opin Micro-biol 29:68–73. https://doi.org/10.1016/j.mib.2015.11.005.

4. Sperandio V. 2018. Pathogens' adaptation to the human host. Proc Natl Acad Sci U S A 115:9342–9343. https://doi.org/10.1073/pnas.1813379115.

5. Garsin DA. 2010. Ethanolamine utilization in bacterial pathogens: roles and regulation. Nat Rev Microbiol 8:290–295. https://doi.org/10.1038/nrmicro2334.

6. Kaval KG, Garsin DA. 2018. Ethanolamine utilization in bacteria. mBio 9: e00066-18. https://doi.org/10.1128/mBio.00066-18.

7. Tsoy O, Ravcheev D, Mushegian A. 2009. Comparative genomics of ethanola-mine utilization. J Bacteriol 191:7157–7164. https://doi.org/10.1128/JB.00838-09.

8. Stojiljkovic I, Bäumler AJ, Heffron F. 1995. Ethanolamine utilization in Salmo-nella typhimurium: nucleotide sequence, protein expression, and mutational analysis of the cchA cchB eutE eutJ eutG eutH gene cluster. J Bacteriol 177:1357–1366. https://doi.org/10.1128/jb.177.5.1357-1366.1995.

9. Chang GW, Chang JT. 1975. Evidence for the B12-dependent enzyme eth-anolamine deaminase in Salmonella. Nature 254:150–151. https://doi .org/10.1038/254150a0.

10. Blackwell CM, Turner JM. 1978. Microbial metabolism of amino alcohols. Formation of coenzyme B12-dependent ethanolamine ammonia-lyase

and its concerted induction in Escherichia coli. Biochem J 176:751–757. https://doi.org/10.1042/bj1760751.

11. Roof DM, Roth JR. 1988. Ethanolamine utilization in Salmonella typhimurium. J Bacteriol 170:3855–3863. https://doi.org/10.1128/jb.170.9.3855-3863.1988.

12. Brinsmade SR, Escalante-Semerena JC. 2004. The eutD gene of Salmonella enterica encodes a protein with phosphotransacetylase enzyme activity. J Bacteriol 186:1890–1892. https://doi.org/10.1128/jb.186.6.1890-1892.2004.

13. Moore TC, Escalante-Semerena JC. 2016. The EutQ and EutP proteins are novel acetate kinases involved in ethanolamine catabolism: physiological implications for the function of the ethanolamine metabolosome in Salmonella enterica. Mol Microbiol 99:497–511. https://doi.org/10.1111/mmi.13243.

14. Price-Carter M, Tingey J, Bobik TA, Roth JR. 2001. The alternative electron acceptor tetrathionate supports B12-dependent anaerobic growth of Salmonella enterica serovar Typhimurium on ethanolamine or 1,2-propanediol. J Bacteriol 183:2463–2475. https://doi.org/10.1128/JB.183.8.2463-2475.2001.

15. Thiennimitr P, Winter SE, Winter MG, Xavier MN, Tolstikov V, Huseby DL, Sterzenbach T, Tsolis RM, Roth JR, Bäumler AJ. 2011. Intestinal inflammation allows Salmonella to use ethanolamine to compete with the microbiota. Proc Natl Acad Sci U S A 108:17480–17485. https://doi.org/10.1073/pnas.1107857108.

16. Stewart KL, Stewart AM, Bobik TA. 6 October 2020. Prokaryotic organelles: bacterial microcompartments in E. coli and Salmonella. EcoSal Plus 2020 https://doi.org/10.1128/ecosalplus.ESP-0025-2019.

17. Light SH, Méheust R, Ferrell JL, Cho J, Deng D, Agostoni M, Iavarone AT, Banfield JF, D'Orazio SE, Portnoy DA. 2019. Extracellular electron transfer powers flavinylated extracellular reductases in Gram-positive bacteria. Proc Natl Acad Sci U S A 116:26892–26899. https://doi.org/10.1073/pnas.1915678116.

18. Light SH, Su L, Rivera-Lugo R, Cornejo JA, Louie A, Iavarone AT, Ajo-Franklin CM, Portnoy DA. 2018. A flavin-based extracellular electron transfer mechanism in diverse Gram-positive bacteria. Nature 562:140–144. https://doi.org/10.1038/s41586-018-0498-z.

19. Kerfeld CA, Aussignargues C, Zarzycki J, Cai F, Sutter M. 2018. Bacterial microcompartments. Nat Rev Microbiol 16:277–290. https://doi.org/10.1038/nrmicro.2018.10.

20. Greening C, Lithgow T. 2020. Formation and function of bacterial organelles. Nat Rev Microbiol 18:677–689. https://doi.org/10.1038/s41579-020-0413-0.

21. Huseby DL, Roth JR. 2013. Evidence that a metabolic microcompartment contains and recycles private cofactor pools. J Bacteriol 195:2864–2879. https://doi.org/10.1128/JB.02179-12.

22. Fan C, Cheng S, Sinha S, Bobik TA. 2012. Interactions between the termini of lumen enzymes and shell proteins mediate enzyme encapsulation into bacterial microcompartments. Proc Natl Acad Sci U S A 109:14995–15000. https://doi.org/10.1073/pnas.1207516109.

23. Kalnins G, Cesle E-E, Jansons J, Liepins J, Filimonenko A, Tars K. 2020. Encapsulation mechanisms and structural studies of GRM2 bacterial microcompartment particles. Nat Commun 11:388. https://doi.org/10.1038/s41467-019-14205-y.

24. Zeng Z, Smid EJ, Boeren S, Notebaart RA, Abee T. 2019. Bacterial microcompartment-dependent 1,2-propanediol utilization stimulates anaerobic growth of Listeria monocytogenes EGDe. Front Microbiol 10:2660. https://doi.org/10.3389/fmicb.2019.02660.

25. Mellin J, Koutero M, Dar D, Nahori M-A, Sorek R, Cossart P. 2014. Sequestration of a two-component response regulator by a riboswitch-regulated noncoding RNA. Science 345:940–943. https://doi.org/10.1126/science.1255083.

26. Kendall MM, Sperandio V. 2016. What a dinner party! Mechanisms and functions of interkingdom signaling in host-pathogen associations. mBio 7:e01748-15. https://doi.org/10.1128/mBio.01748-15.

27. Tang S, Orsi RH, den Bakker HC, Wiedmann M, Boor KJ, Bergholz TM. 2015. Transcriptomic analysis of the adaptation of Listeria monocytogenes to growth on vacuum-packed cold smoked salmon. Appl Environ Microbiol 81:6812–6824. https://doi.org/10.1128/AEM.01752-15.

28. Anast JM, Schmitz-Esser S. 2020. The transcriptome of Listeria monocytogenes during co-cultivation with cheese rind bacteria suggests adaptation by induction of ethanolamine and 1,2-propanediol catabolism pathway genes. PLoS One 15:e0233945. https://doi.org/10.1371/journal.pone.0233945.

29. Joseph B, Przybilla K, Stühler C, Schauer K, Slaghuis J, Fuchs TM, Goebel W. 2006. Identification of Listeria monocytogenes genes

30. Anderson CJ, Clark DE, Adli M, Kendall MM. 2015. Ethanolamine signaling promotes Salmonella niche recognition and adaptation during infection. PLoS Pathog 11:e1005278. https://doi.org/10.1371/journal.ppat.1005278.

31. Tsai H-N, Hodgson DA. 2003. Development of a synthetic minimal medium for Listeria monocytogenes. Appl Environ Microbiol 69:6943–6945. https://doi.org/10.1128/aem.69.11.6943-6945.2003.

32. Feehily C, O'Byrne CP, Karatzas KAG. 2013. Functional γ-aminobutyrate shunt in Listeria monocytogenes: role in acid tolerance and succinate biosynthesis. Appl Environ Microbiol 79:74–80. https://doi.org/10.1128/AEM.02184-12.

33. Lebreton A, Cossart P. 2017. RNA- and protein-mediated control of Listeria monocytogenes virulence gene expression. RNA Biol 14:460–470. https://doi.org/10.1080/15476286.2016.1189069.

34. Li Z, Pérez-Osorio A, Wang Y, Eckmann K, Glover WA, Allard MW, Brown EW, Chen Y. 2017. Whole genome sequencing analyses of Listeria monocytogenes that persisted in a milkshake machine for a year and caused illnesses in Washington State. BMC Microbiol 17:134. https://doi.org/10.1186/s12866-017-1043-1.

35. Lobel L, Sigal N, Borovok I, Ruppin E, Herskovits AA. 2012. Integrative genomic analysis identifies isoleucine and CodY as regulators of Listeria monocytogenes virulence. PLoS Genet 8:e1002887. https://doi.org/10.1371/journal.pgen.1002887.

36. Cheng S, Sinha S, Fan C, Liu Y, Bobik TA. 2011. Genetic analysis of the protein shell of the microcompartments involved in coenzyme B12-dependent 1,2-propanediol degradation by Salmonella. J Bacteriol 193:1385–1392. https://doi.org/10.1128/JB.01473-10.

37. Dadswell K, Creagh S, McCullagh E, Liang M, Brown IR, Warren MJ, McNally A, MacSharry J, Prentice MB. 2019. Bacterial microcompartment-mediated ethanolamine metabolism in Escherichia coli urinary tract infection. Infect Immun 87:e00211-19. https://doi.org/10.1128/IAI.00211-19.

38. Kaval KG, Gebbie M, Goodson JR, Cruz MR, Winkler WC, Garsin DA. 2019. Ethanolamine utilization and bacterial microcompartment formation are subject to carbon catabolite repression. J Bacteriol 201:e00703-18. https://doi.org/10.1128/JB.00703-18.

39. Pang A, Warren MJ, Pickersgill RW. 2011. Structure of PduT, a trimeric bacterial microcompartment protein with a 4Fe-4S cluster-binding site. Acta Crystallogr D Biol Crystallogr 67:91–96. https://doi.org/10.1107/S0907444910050201.

40. Ferlez B, Sutter M, Kerfeld CA. 2019. Glycyl radical enzyme-associated microcompartments: redox-replete bacterial organelles. mBio 10:e02327-18. https://doi.org/10.1128/mBio.02327-18.

41. Singh S, Brocker C, Koppaka V, Chen Y, Jackson BC, Matsumoto A, Thompson DC, Vasiliou V. 2013. Aldehyde dehydrogenases in cellular responses to oxidative/electrophilic stress. Free Radic Biol Med 56:89–101. https://doi.org/10.1016/j.freeradbiomed.2012.11.010.

42. McLaughlin HP, Hill C, Gahan CG. 2011. The impact of iron on Listeria monocytogenes; inside and outside the host. Curr Opin Biotechnol 22:194–199. https://doi.org/10.1016/j.copbio.2010.10.005.

43. Portman JL, Dubensky SB, Peterson BN, Whiteley AT, Portnoy DA. 2017. Activation of the Listeria monocytogenes virulence program by a reducing environment. mBio 8:e01595-17. https://doi.org/10.1128/mBio.01595-17.

44. Smith K, Youngman P. 1992. Use of a new integrational vector to investigate compartment-specific expression of the Bacillus subtilis spoIIM gene. Biochimie 74:705–711. https://doi.org/10.1016/0300-9084(92)90143-3.

45. Reynolds AJ, Verheyen TV, Adeloju SB, Chaffee A, Meuleman E. 2014. Quantification of aqueous monoethanolamine concentration by gas chromatography for postcombustion capture of CO2. Ind Eng Chem Res 53:4805–4811. https://doi.org/10.1021/ie404157p.

46. Wiśniewski JR, Zougman A, Nagaraj N, Mann M. 2009. Universal sample preparation method for proteome analysis. Nat Methods 6:359–362. https://doi.org/10.1038/nmeth.1322.

47. Smaczniak C, Immink RGH, Muiño JM, Blanvillain R, Busscher M, Busscher-Lange J, Dinh QDP, Liu S, Westphal AH, Boeren S, Parcy F, Xu L, Carles CC, Angenent GC, Kaufmann K. 2012. Characterization of MADS-domain transcription factor complexes in Arabidopsis flower development. Proc Natl Acad Sci U S A 109:1560–1565. https://doi.org/10.1073/pnas.1112871109.

48. Tyanova S, Temu T, Sinitcyn P, Carlson A, Hein MY, Geiger T, Mann M, Cox J. 2016. The Perseus computational platform for comprehensive analysis

of (prote)omics data. Nat Methods 13:731–740. https://doi.org/10.1038/nmeth.3901.

49. Drozdetskiy A, Cole C, Procter J, Barton GJ. 2015. JPred4: a protein secondary structure prediction server. Nucleic Acids Res 43:W389–W394. https://doi.org/10.1093/nar/gkv332.

50. Hulsen T, de Vlieg J, Alkema W. 2008. BioVenn—a Web application for the comparison and visualization of biological lists using area-proportional Venn diagrams. BMC Genomics 9:488. https://doi.org/10.1186/1471-2164-9-488.

51. Szklarczyk D, Gable AL, Lyon D, Junge A, Wyder S, Huerta-Cepas J, Simonovic M, Doncheva NT, Morris JH, Bork P, Jensen LJ, von Mering C. 2019. STRING v11: protein-protein association networks with increased coverage, supporting functional discovery in genome-wide experimental datasets. Nucleic Acids Res 47:D607–D613. https://doi.org/10.1093/nar/gky1131.